

Studies of heavy-ion collisions using PYTHIA Angantyr and UrQMD

André Vieira da Silva,¹ Willian Matioli Serenone,¹ David
Dobrigkeit Chinellato,¹ Jun Takahashi,¹ and Christian Bierlich^{2,*}

¹*Universidade Estadual de Campinas, São Paulo, Brazil*

²*Dept. of Astronomy and Theoretical Physics, Lund University, Sweden*

(Dated:)

In this paper, we show predictions from a new QGP-free, no-equilibration, improved baseline model for heavy-ion collisions. It is comprised of the PYTHIA/Angantyr event generator coupled to UrQMD, as a hadronic cascade simulator, and compared to ALICE and CMS data from Pb-Pb collisions at $\sqrt{s_{\text{NN}}} = 2.76$ TeV. This coupling is made possible due to a new implementation of the hadron vertex model in PYTHIA/Angantyr. Hadronic rescattering in UrQMD is shown to lead to a significant suppression of mid- to high- p_{\perp} particle yields that is qualitatively consistent with measurements of nuclear modification factors. We further study the effect of hadronic rescatterings on high- p_{\perp} particles by using two-particle correlations and show that some suppression of away-side jets occurs in the hadronic phase even without any partonic energy loss. Finally, the decorrelation of dijet structures at high momenta also leads to a reduction of the elliptic flow coefficient $v_2\{2\}$. These findings suggest that significant jet-quenching-like effects may still originate in the hadronic, as opposed to the partonic phase and prove that the usual Pb-Pb baseline, composed of a superposition of incoherent pp collisions, ignores coherent phenomena that are not strictly related to the QGP but may still be highly relevant.

The ultra-relativistic heavy ion (AA) collisions, measured at the LHC and RHIC experiments, produce the hottest, densest state of matter available in a laboratory. Such collisions are expected to lead to a deconfined state of quarks and gluons, denoted the Quark–Gluon Plasma (QGP) [1–4]. Several signatures of this phase of matter have been found in AA collisions. Notably, the yields of high- p_{\perp} particles are suppressed with respect to expectations from scaled proton–proton (pp) collisions [5], away-side jets are suppressed in central AA collisions [6, 7] and particles are emitted anisotropically in azimuth because of collective flow developed during the system evolution [8].

Recently, effects normally associated with the formation of a QGP phase, such as multi-particle flow [9] and enhanced strangeness production [10], were also observed in pp collisions. The discovery that the demarcation between QGP-producing and no-QGP-producing collision systems is not as clear as previously thought, should naturally lead to questions regarding the no-QGP baseline used in jet quenching searches in AA collisions. Not only is it unclear that a given pp collision can be taken as a pure baseline result, it is also unclear that an AA collision can be taken as a simple superposition of pp collisions, even without considering QGP effects. It has recently been shown by the ALICE experiment [11] that the charged-particle multiplicity in very central AA collisions breaks the scaling with number of participating nucleons. Furthermore, a correct description of basic quantities must take into account effects not arising from the QGP phase, but rather from nuclear shadowing

or diffractive contributions. Additionally, it is well known that, compared to pp collisions, the large geometry of an AA collision also potentially allows hadronic rescattering effects to affect relative production rates and kinematics [12], another effect in AA collisions not linked to QGP production. In this work, we present an improved, QGP-free baseline for heavy-ion collisions to replace the traditional incoherent superposition of pp collisions. This effort is crucially important to disentangle effects that are exclusively due to the QGP. Special emphasis will be given to the mid- to high p_{\perp} region $p_{\perp} > 4$ GeV/ c .

In the traditional heavy-ion picture, high- p_{\perp} particles will be sensitive to partonic energy loss while traversing the QGP and a modification of the high- p_{\perp} yield in AA collisions compared to pp collisions is generally taken as a sign of a QGP phase. This is quantified by the nuclear modification factor:

$$R_{AA} = \frac{d^2 N_{\text{ch}}/dp_{\perp} dy|_{AA}}{N_{\text{coll}} d^2 N_{\text{ch}}/dp_{\perp} dy|_{pp}}, \quad (1)$$

where y is the rapidity and N_{coll} is a scaling factor corresponding to the number of binary nucleon–nucleon collisions calculated using the Glauber model [13, 14].

The standard picture of high- p_{\perp} modification can be phrased in terms of the QGP transport coefficient, which denotes the broadening of the transverse momentum distribution per unit length $\hat{q} = \langle p_{\perp}^2 \rangle_L / L$. According to a selection of the models implemented in the JETSCAPE generator framework [15], a high virtuality $Q^2 \gg \sqrt{\hat{q}E}$ (where E is the parton energy) parton will undergo a medium-modified DGLAP evolution [16] and at lower Q^2 the shower modifications can be calculated by transport theory [17, 18]. The JEWEL

* Also at: Niels Bohr Institute, University of Copenhagen, Denmark

approach [19] treats high to intermediate virtuality by a combination of partonic rescattering and the Landau-Pomeranchuk-Migdal effect [20]. In both cases the relevant degrees of freedom are partonic.

Dynamical models based on perturbative QCD coupled to either string or cluster hadronization [21, 22] have worked very well to describe most features of e^+e^- , ep and pp collisions. Such models are implemented in so-called General Purpose Monte Carlo event generators, of which PYTHIA 8.2 [23], HERWIG 7 [24] or SHERPA [25] are prominent examples. The PYTHIA model for multiparton interactions (MPIs) [26] has recently been extended to heavy ion collisions, and the resulting PYTHIA/Angantyr [27, 28] is a QGP-free simulation of heavy ion collisions that includes the contributions mentioned above. For the final state hadronic interactions, quantum molecular dynamics models such as UrQMD [12, 29] and more recently SMASH [30] have worked very well in hybrid approaches together with hydrodynamics for modelling QGP created in heavy ion collisions [31], in air-shower simulations [32] as well as detector simulations [33]. In this paper we present a hybrid approach linking PYTHIA/Angantyr+UrQMD to model a realistic, QGP free final state of a heavy ion collision.

I. MODEL SETUP

The PYTHIA/Angantyr+UrQMD hybrid model is outlined in Fig. 1. On the right side of the figure, the standard view on a heavy ion collision is sketched. Importantly, this includes the formation of a strongly coupled, nearly thermal QGP phase. This phase can be described by relativistic hydro-

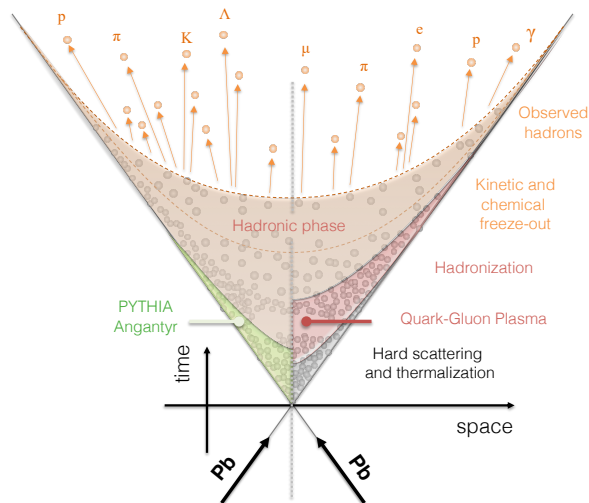


Figure 1. Schematic representation of the modeling of a heavy-ion collision using the usual approach (right side of the figure) and the PYTHIA/Angantyr+UrQMD no-QGP baseline method (left side of the figure).

dynamics [34], and is observed to “quench” jets by comparing the single particle yields at high p_\perp to that of pp collisions. The alternative, QGP free, description is sketched on the left side of Fig. 1. Instead of assuming the formation of a QGP, that part of the evolution is carried out using just the PYTHIA/Angantyr model, which will be presented below. The right and left sides of Fig. 1 share the final phase of the evolution, consisting of hadronic interactions.

The PYTHIA model for MPIs

In a pp collision, MPIs are generated under the assumption that different partonic interactions are almost independent [35]. As such, MPIs are selected according to the $2 \rightarrow 2$ perturbative parton-parton cross section:

$$\frac{d\sigma_{2 \rightarrow 2}}{dp_\perp^2} \propto \frac{\alpha_s^2(p_\perp^2)}{p_\perp^4} \rightarrow \frac{\alpha_s^2(p_\perp^2 + p_{\perp 0}^2)}{(p_\perp^2 + p_{\perp 0}^2)^2}. \quad (2)$$

Since the cross section diverges like $1/p_\perp^4$, it is regularised using a parameter $p_{\perp 0}$. This value can be interpreted as being proportional to the inverse of a maximal (colour) screening length of a proton. MPIs are interleaved [36] with the initial state and final state parton showers (ISR and FSR, where ‘R’ stands for radiation), which are also ordered in p_\perp . This implies that MPIs, ISR and FSR obey a combined evolution equation that determines the p_\perp of the next step in the evolution, whether that is the generation of a new MPI, and ISR or an FSR emission.

The final step before hadronization concerns color reconnection of partonic systems. The idea originates in the notion that having many MPIs leads to many color strings, which moving from the $N_c \rightarrow \infty$ limit to $N_c = 3$, can be connected in many different ways. Since nature is expected to favour configurations with the lowest potential energy – and thus the smallest total string length – this is the guiding principle for present models. The current default model for color reconnection, the one used in this paper, gives each MPI system a probability to reconnect with a harder system which is:

$$\mathcal{P} = \frac{p_{\perp \text{Rec}}^2}{p_{\perp \text{Rec}}^2 + p_\perp^2}, \quad p_{\perp \text{Rec}} = R \times p_{\perp 0}, \quad (3)$$

where R is a tunable parameter, and $p_{\perp 0}$ is the same parameter as in Eq. (2). This makes it easier to connect low- p_\perp systems with high p_\perp ones, essentially making high- p_\perp systems “sweep up” some of the low- p_\perp ones.

PYTHIA/Angantyr for heavy ion collisions

In a heavy ion collision, each (projectile) nucleon can interact with several (target) nucleons. The

amount of interacting nucleons can be determined by a Glauber model, to which PYTHIA/Angantyr makes several additions. Most importantly, for this paper, there is a distinction between different types of nucleon–nucleon interactions: elastic, diffractive and absorptive (ie. inelastic, non-diffractive) sub-collisions. In PYTHIA/Angantyr this is done by parametrizing the nucleon–nucleon elastic amplitude in impact parameter space ($T(\vec{b})$), and its fluctuations. Details of the parametrization can be studied in ref. [28], but crucially, it allows for a) determination of all parameters from fits to semi-inclusive pp cross sections, and b) calculation of the amplitude $T_{kl}(b)$ for any combination of projectile state k and target state l . Once it is determined which nucleons *may* interact and their type of interaction, it is then determined if they *will* interact, and, for absorptive sub-collisions, if the interaction will be considered *primary* or *secondary*. This final distinction is based on the wounded nucleon model [37], according to which a wounded nucleon in a pA or AA collision contributes to the final state multiplicity as:

$$\frac{dN_{\text{ch}}}{d\eta} = w_p F(\eta) + w_t F(-\eta), \quad (4)$$

where w_i denotes the number of wounded nucleons in projectile and target respectively, and $F(\eta)$ is a single-nucleon emission function (of pseudo-rapidity). For a pp collision $w_p = w_t = 1$. A proton–deuteron collision, with all nucleons wounded, will thus reduce to a pp collision, plus an additional wounded nucleon contributing only on the deuteron side. In the language of PYTHIA/Angantyr: one *primary* absorptive collision and one *secondary* absorptive collision. The primary collision is modelled as a normal inelastic, non-diffractive collision, whereas the secondary absorptive one is treated with inspiration from the Fritiof model [38]. In Fritiof, a single string with a mass distribution $\propto dM^2/M^2$, similar to diffractive excitation, was used. In PYTHIA/Angantyr such sub-systems are allowed to have MPIs in secondary collisions, following the interleaved MPI/shower prescription described above. This procedure can be generalized to an arbitrary AA collision. In PYTHIA/Angantyr this is done by first ordering all possible interaction in increasing local impact parameter. Going from smallest to largest impact parameter, an interaction is labelled primary if neither of the participating nucleons have participated in a previous interaction and secondary otherwise.

On the conceptual level, there are some differences between pp events generated with the PYTHIA 8.2 MPI model and pA or AA events generated with the PYTHIA/Angantyr model. Most importantly, color reconnection is in PYTHIA/Angantyr only applied at the level of individual nucleon–nucleon collisions. As seen from Eq. (3), the current color reconnection model in-

cludes no dependence on impact parameter, but has instead the implicit assumption that a soft MPI will have a large spatial spread, and thus be easier to reconnect. While this may be reasonable for a pp collision where everything is confined to the transverse size of a single nucleon, it is inappropriate for heavy ion collisions. In that case, possible reconnections across separate nucleon–nucleon interactions are therefore neglected altogether. Other more recent developments in string models, such as color ropes [39] and string shoving [40], are also not considered in this work. While both effects would be interesting to study with the scope of constructing a full, microscopic alternative to the QGP, the goal here is rather to demonstrate the behaviour of heavy ion collisions considering no parton level QGP-like interactions. Furthermore the concept of interleaved evolution is also only followed for individual nucleon–nucleon collisions, and not the full AA collision.

Hadron production vertices

After construction of a parton-level event, as outlined above, the color reconnected strings hadronize. This is done using the Lund string hadronization model [21, 41–43], as implemented in PYTHIA 8.2. A string represents the gluonic flux tube stretched between a quark–anti-quark pair. At distances larger than ≈ 1 fm, the confinement potential is linear $V(r) = \kappa r$, with the string tension $\kappa \approx 1$ GeV/fm, cf. lattice calculations [44]. As the string grows, energy is transferred from endpoint momenta to potential energy until the string breaks into hadrons [45]. A crucial feature of the Lund model is that the string hadronization time, in the string rest frame, can be calculated. This time signifies directly the end of the pre-hadronic phase, and start of the hadronic cascade. The hadronization time follows a Gamma distribution with the average:

$$\langle \tau^2 \rangle = \frac{1+a}{b\kappa^2}. \quad (5)$$

The two parameters a and b also enters the Lund symmetric fragmentation function, which determines the longitudinal momentum fraction taken away from the string by each hadron. As such, they are strongly correlated with total charged multiplicity and momentum fraction, and can be fitted to e^+e^- collider data. The standard values [46] gives $\langle \tau^2 \rangle \approx 2$ fm/c. In order to couple the output from PYTHIA/Angantyr to UrQMD, space-time information of hadron production vertices is necessary. It was recently shown [47] that production vertices of even complicated multi-parton systems can be extracted in the Lund model and implemented in PYTHIA 8.2. The key component of this translation comes from noting that the linear confinement potential gives rise to a linear rela-

relationship between space-time and momentum quantities. The space-time location of a string breakup vertex on a simple $q\bar{q}$ string can therefore be defined as:

$$v = \frac{x^+ p^+ + x^- p^-}{\kappa}, \quad (6)$$

where p^\pm are the q and \bar{q} four-momenta, and x^\pm are (normalized) light-cone coordinates of the break-up point. The production vertex of the hadron is then taken to be the average of the two break-up vertices producing it. It should be stressed that this simple explanation of a $q\bar{q}$ system does not give justice to the many complications arising from treatment of multi-parton geometries, gluon loops, massive quarks or junction topologies, but the reader is referred to ref. [47] for details about complicated systems.

The application to PYTHIA/Angantyr is straightforward. In each nucleon–nucleon collision, each MPI parton is assigned a primordial vertex randomly from the overlap of two 2D Gaussian distributions (the nucleon mass distribution), and each nucleon assigned an overall position in the event according to the initial Glauber simulation.

Coupling to UrQMD

Immediately after hadronization, 99.8% of all particles are propagated using UrQMD 3.4 and may interact elastically and inelastically or decay if unstable, while the remaining 0.2% are treated separately due to technical limitations. Since hadrons containing charm quarks, which correspond to approximately 0.2% of all produced particles, are not adequately treated by UrQMD, these particles are exceptionally decayed by PYTHIA and only their decay products are used in the hadronic cascade simulation. Photons and leptons make up 0.01% of all particles produced by PYTHIA/Angantyr and are discarded prior to the simulation of the hadronic phase as they would not be recognized or not interact in UrQMD.

A notable difference in this coupling, compared to the usual application of UrQMD with hydrodynamics-based event generators, is that the latter evolve the system by $\mathcal{O}(10 \text{ fm}/c)$, while PYTHIA/Angantyr provides a significant fraction of final hadrons already after 1-2 fm/c after the initial hard scatterings even in central collisions, as can be seen in Fig. 2. Another significant distinction is that, while hydrodynamics-based simulation chains produce hadrons at a particlization surface, PYTHIA/Angantyr provides a position distribution over a three-dimensional volume and considers jet-like physical correlations between space and time that are not taken into account in hydro-based models. Remarkably, in this model, small- p_\perp

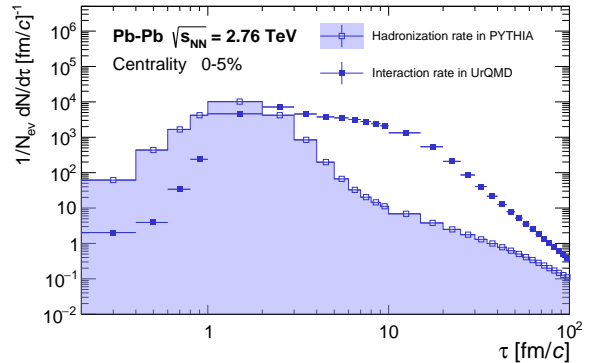


Figure 2. Time $\tau = \sqrt{t^2 - z^2}$ distribution of hadrons created by PYTHIA/Angantyr in 0-5% central Pb-Pb collisions at 2.76 TeV shown together with the time distribution of UrQMD scatterings (solid symbols).

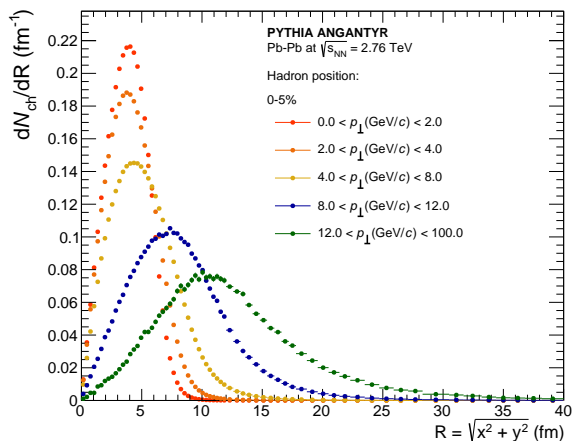


Figure 3. Transverse radius R distribution of hadrons created by PYTHIA/Angantyr in 0-5% central Pb-Pb collisions at 2.76 TeV for various transverse momentum ranges.

hadrons are all created at low radii in central Pb-Pb collisions, high- p_\perp hadrons will have their production vertices offset from the nucleon–nucleon collision, as can be seen in Fig. 3. Ultimately, all these effects lead to an average hadron density in PYTHIA/Angantyr that is approximately 2-3 times larger than the one observed in hydrodynamic simulations and the resulting hadronic phase lasts significantly longer, as can be seen in the hadron interaction time distribution in Fig. 2. Therefore, the effects of hadronic interactions may be more significant in the PYTHIA/Angantyr+UrQMD simulation chain compared to hydrodynamics-based models.

In order to study simulated events as a function of collision centrality, a number of different options, such as selecting on impact parameter or charged-particle multiplicity in different rapidity ranges, were considered. These options are

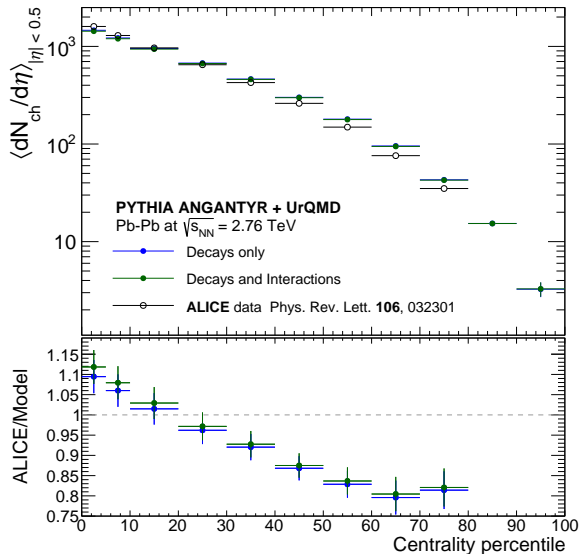


Figure 4. Charged-particle multiplicity density as a function of centrality in Pb-Pb collisions at 2.76 TeV from PYTHIA/Angantyr+UrQMD simulations with and without hadronic scattering compared to ALICE data [48].

found to be largely consistent within 0-70% centrality. The analysis is performed with centrality estimated using charged-particle multiplicities calculated for the rapidity range $-3.7 < \eta < -1.7$ and $2.8 < \eta < 5.1$, corresponding to the acceptance of the VOM detector of the ALICE experiment and therefore matching what is done in real data analysis. All results presented in what follows were produced using a sample of 10^7 Pb-Pb collisions at $\sqrt{s_{NN}} = 2.76$ TeV generated with the PYTHIA/Angantyr+UrQMD simulation chain.

II. RESULTS

The charged-particle multiplicity density obtained with the full PYTHIA/Angantyr+UrQMD simulation is within approximately 20% of the corresponding ALICE measurements [48], as shown in Fig. 4. In order to isolate the effect coming from hadronic scattering, the simulation is also re-run with interactions disabled, leading to no more than a 2-3% difference in charged-particle multiplicity densities and therefore no significant change in how simulations compare to data.

A. Particle spectra and R_{AA}

The effect of the hadronic phase can be further characterized by calculating the p_{\perp} distributions of charged particles, shown in Fig. 5 for various centrality classes.

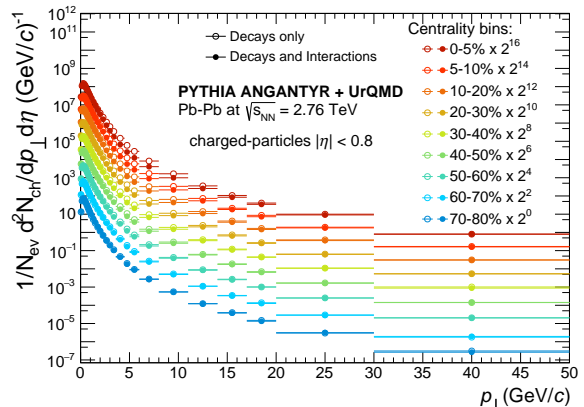


Figure 5. Transverse momentum distributions of charged particles in Pb-Pb collisions at 2.76 TeV simulated with PYTHIA/Angantyr+UrQMD.

The effect of hadronic interactions can be quantified by calculating the ratio of the p_{\perp} distributions obtained with and without scatterings, as seen in Fig. 6. While yields are modified by no more than 10-15% below 2 GeV/c, the effect is more pronounced at mid- to high- p_{\perp} , with a maximum suppression of 60% taking place at approximately 5 GeV/c for 0-10% collisions. The suppression due to hadronic interactions becomes progressively smaller for higher p_{\perp} , and more peripheral collisions.

It should be noted here that the main model uncertainty related to coupling PYTHIA/Angantyr to UrQMD lies in the determination of the vertex position. The relation in Eq. (6) leads directly to a hadron production point as the average of two subsequent break-up points. As noted in ref. [47], this definition is not unique, but could differ from the average up to $\pm p_h/2\kappa$, where p_h is the hadron four-momentum. Taking this at face value, the uncertainty of the modification shown in Fig. 6 is of up to approximately $\pm 50\%$ of the fractional values. While this value is probably an overestimate of the real uncertainty, as very extreme definitions were considered, this result also indicates that further theoretical work may still be needed to constrain hadron creation vertices.

The results seen in Fig. 6 are reminiscent of the suppression of high- p_{\perp} particles seen in the nuclear modification factor R_{AA} . To calculate the R_{AA} from the PYTHIA/Angantyr+UrQMD model, pp collisions were generated using the exact same settings and simulation chain and the average number of binary collisions N_{coll} is assumed to be the one calculated by the ALICE Collaboration using the Glauber model [50]. The simulated R_{AA} with and without hadronic interactions can be seen in Fig. 7 for Pb-Pb at $\sqrt{s_{NN}} = 2.76$ TeV, respectively, for two selected centrality classes. With interactions disabled, the model overestimates the R_{AA} at mid- p_{\perp} , from 4 GeV/c to 10 GeV/c for periph-

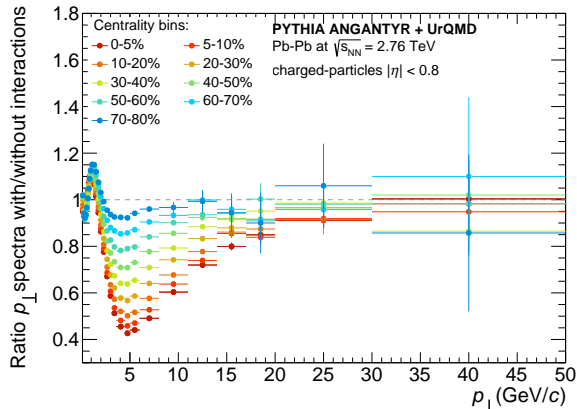


Figure 6. Ratio of charged particle p_{\perp} distributions with and without hadronic interactions in Pb-Pb collisions at 2.76 TeV simulated with PYTHIA/Angantyr+UrQMD in various centrality classes.

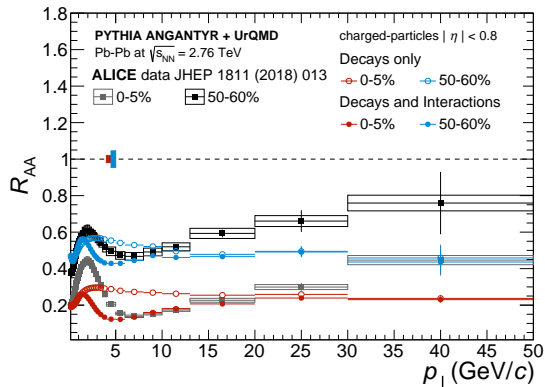


Figure 7. Nuclear modification factor (R_{AA} in mid-central and central collisions in Pb-Pb at $\sqrt{s_{NN}} = 2.76$ TeV in PYTHIA/Angantyr+UrQMD with and without hadronic interactions compared to data from the ALICE experiment [49].

eral collisions and 4 GeV/c to 20 GeV/c for the most central collisions. When hadronic interactions are enabled, there is a further suppression of R_{AA} in these p_{\perp} regions, improving the agreement of our simulation with the observed experimental data in the p_{\perp} range. At higher momenta, however, PYTHIA/Angantyr+UrQMD fails to describe the data, underpredicting the R_{AA} significantly. Notably, had we normalized the R_{AA} differently, such that the result from PYTHIA/Angantyr should converge to unity at high momenta, then the modification observed when enabling UrQMD would lead to a yield suppression that is not strong enough to reproduce the measured R_{AA} . This indicates that there is no trivial change to the calculation that would lead to a correct simultaneous reproduction of the charged-particle multiplicity densities and an R_{AA} that converges to unity at high p_{\perp} .

This is due to PYTHIA/Angantyr+UrQMD being based on the wounded nucleon model, and thus having no concept of N_{coll} scaling built in. From basic factorization arguments, it is clear that at some scale $p_{\perp,sep}$, N_{coll} scaling is expected. The numerical value of this separation scale between the hard and the soft component can, however, not be inferred directly. In the seminal paper by Eskola *et al.* [51], a value of $p_{\perp,sep} = 2$ GeV/c was used, while other contemporary approaches, such as Fritiof [38] or by Ranft [52], would place the value higher, in line with the results shown in this paper. The significance of the results shown in Fig. 7 can thus be interpreted differently, depending on one's choice of $p_{\perp,sep}$. If $p_{\perp,sep}$ is as small as 2 GeV/c, the PYTHIA/Angantyr+UrQMD baseline is wrong down to that value. Regardless of the baseline, Fig. 7 shows that a hadronic cascade can significantly impact R_{AA} with up to 50%, but the agreement between simulation and data up to around $p_{\perp} = 15$ GeV/c is, with this choice of $p_{\perp,sep}$, merely co-incidental [53]. On the other hand, if $p_{\perp,sep}$ is higher, and the hard component starts taking over at values as high as $p_{\perp} \gtrsim 15 - 20$ GeV/c, the result in Fig. 7 suggests that no QGP modification of high- p_{\perp} partons is necessary to describe R_{AA} up to around that value, and that R_{AA} is therefore *not* a good observable to study medium modifications in the intermediate p_{\perp} range.

B. Two-particle correlation study

To further understand the nature of the high- p_{\perp} yield suppression, we performed two-particle correlation (2PC) studies using a high- p_{\perp} trigger range of 6 to 8 GeV/c and an associated trigger range of 4 to 6 GeV/c, corresponding to the region of maximum suppression observed in Fig. 6. The correlation function $C(\Delta\phi, \Delta\eta)$ is calculated for particles within $|\eta| < 2.5$ and is defined as

$$C_{full}(\Delta\phi, \Delta\eta) = \frac{C_{same}(\Delta\phi, \Delta\eta)}{\alpha \times C_{mixed}(\Delta\phi, \Delta\eta)}, \quad (7)$$

where C_{same} denotes the correlation function calculated with pairs from the same event and C_{mixed} is calculated for particles from different events, following the ‘mixed event’ technique. This technique corrects for limited pair acceptance, and is often used by experiments. It is used here in order to repeat the analysis in the same way as an experiment would perform it. Events are only mixed if they differ in centrality by no more than 2% and C_{mixed} is populated using at least 500 unrelated events for each single event being processed. The normalization factor α is chosen such that $C_{mixed}(\Delta\phi, \Delta\eta)$ is unity at $\Delta\eta = 0$, indicating that particles having the same η value will always be accepted by the $|\eta| < 2.5$ acceptance cut and be paired successfully. Furthermore, uncorrelated background in C

is calculated using the mixed event technique as well, though for that case events are mixed after rotating them such that their event planes (EPs), defined as the plane constructed out of the beam axis and the vector connecting the two nuclei centers in the transverse plane, are aligned. The background to be subtracted from $C(\Delta\phi, \Delta\eta)$ is then calculated using

$$C_{\text{bg}}(\Delta\phi, \Delta\eta) = \frac{\beta \times C_{\text{mixed}}^{\text{aligned EP}}(\Delta\phi, \Delta\eta)}{\alpha \times C_{\text{mixed}}(\Delta\phi, \Delta\eta)}, \quad (8)$$

where α and C_{mixed} are the same as in Eq. (7), $C_{\text{mixed}}^{\text{aligned EP}}$ is the mixed-event correlation function calculated with aligned EPs and β is a normalization factor to account for imperfections in the mixed-event background estimate. The factor β is calculated by matching the particle yield of C_{bg} to that of C_{full} in the near-side region but away from the peak, sampled in $1.0 < |\Delta\eta| < 4.0$ and $|\Delta\phi| < \pi/2$. The final, background-subtracted correlation function is then defined simply as:

$$C(\Delta\phi, \Delta\eta) = C_{\text{full}}(\Delta\phi, \Delta\eta) - C_{\text{bg}}(\Delta\phi, \Delta\eta) \quad (9)$$

This subtraction method is perfectly suited to remove elliptic-flow-like correlations, which are in fact present in this model as discussed in the next section, and any imperfections and higher-order corrections have been tested to be negligible in the momentum ranges considered in this study.

This procedure was repeated for all centralities analysed before and the results of the projection of $C(\Delta\phi, \Delta\eta)$ onto $\Delta\phi$ are shown in Fig. 8 in a few selected centrality classes. A small, but still significant, suppression of the away-side jet structure can be observed when hadronic interactions are enabled, while the near-side yields are only minimally affected even in central events and match those observed in peripheral collisions. This is an indication that the hadronic interactions are such that an outgoing trigger particle is likely to be closer to the edge of the heavy-ion collision, in which case the corresponding away-side jet structure will undergo significant interaction with the remainder of the system.

This observation is qualitatively reminiscent of measurements performed at RHIC by STAR in which dijets were studied using 2PC and the away side was completely suppressed in central collisions [6, 7]. In that case, the explanation of this phenomenon was also related to the outgoing trigger particle being away from the center of the collision, but the suppression of the away side was seen as a consequence of partonic rather than hadronic interactions. However, it is worth noting that though qualitatively consistent, the overall magnitude of the effect observed in our model is smaller than the one required to achieve a full suppression of the away side.

To quantify the magnitude of the yield loss in the away side as a function of centrality, we inte-

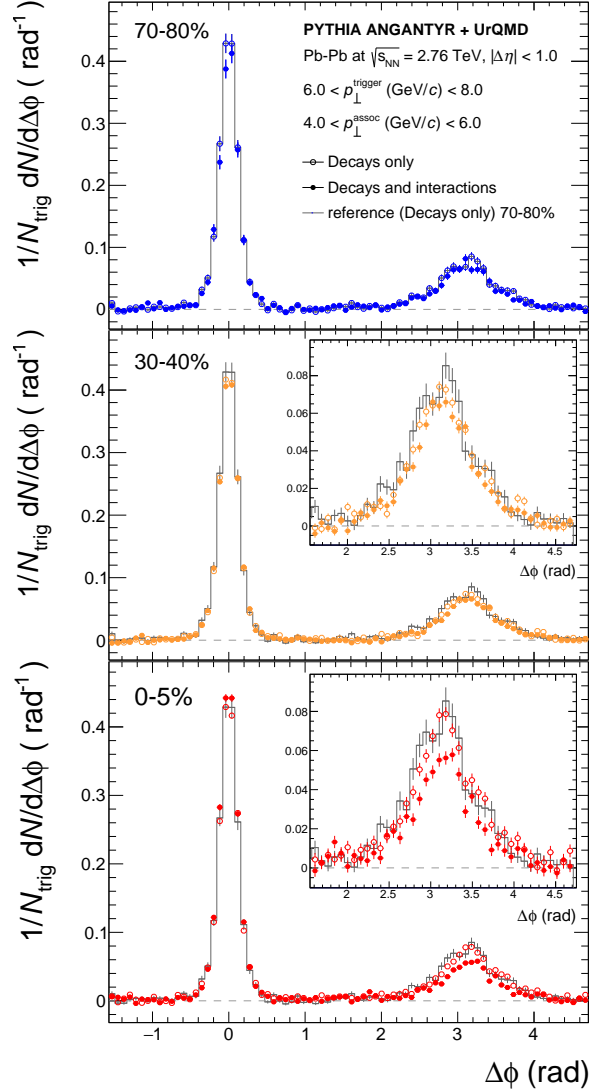


Figure 8. Two-particle correlation in $\Delta\phi$ using $6.0 < p_{\perp}^{\text{trigger}} \text{ (GeV}/c) < 8.0$ and $4.0 < p_{\perp}^{\text{assoc}} \text{ (GeV}/c) < 6.0$ in three selected event classes in Pb-Pb at $\sqrt{s_{\text{NN}}} = 2.76 \text{ TeV}$ in PYTHIA/Angantyr+UrQMD with and without hadronic interactions.

grate the background-subtracted correlation function $C(\Delta\phi, \Delta\eta)$ in the near side, $-\pi/2 < \Delta\phi < +\pi/2$, and in the away side, $+\pi/2 < \Delta\phi < +3\pi/2$, with and without hadronic interactions and then plot the ratio of these two configurations in Fig. 9. While the near-side jet yield is independent of centrality, the away-side yield is progressively suppressed with centrality, reaching a maximum suppression of approximately 30% for 0-5% Pb-Pb events.

The reason for the observed dynamics can be further explored by calculating the average number of hadronic collisions $\langle N_{\text{coll}}^{\text{hadronic}} \rangle$ as a function of $\Delta\phi$, as seen in Fig. 10. It is revealed that the $\langle N_{\text{coll}}^{\text{hadronic}} \rangle$ is significantly smaller around $\Delta\phi \approx 0$, indicating that the triggered near-side jet leaves

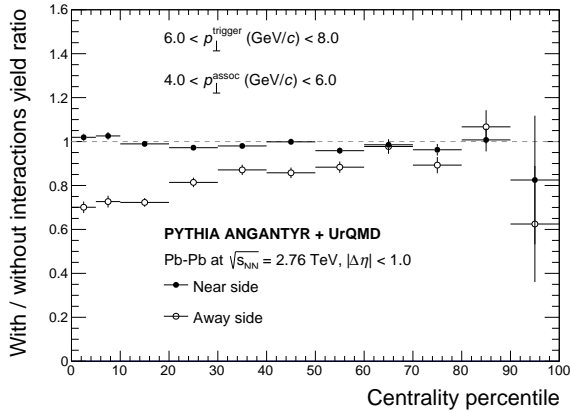


Figure 9. Jet yield modification for the away- and near-side jets as a function of centrality in Pb-Pb at $\sqrt{s_{NN}} = 2.76$ TeV in PYTHIA/Angantyr+UrQMD with and without hadronic interactions.

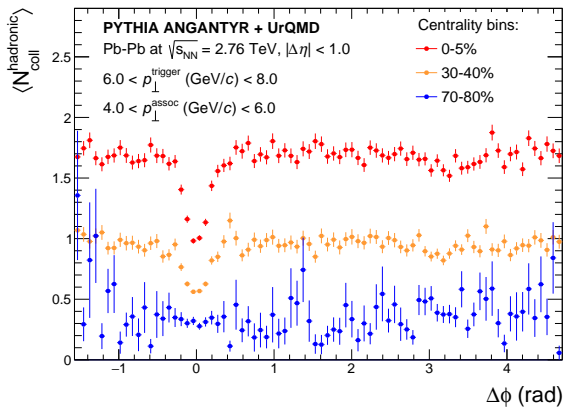


Figure 10. Average number of hadronic collisions as a function of $\Delta\phi$ in three selected event class in Pb-Pb at $\sqrt{s_{NN}} = 2.76$ TeV in PYTHIA/Angantyr+UrQMD with and without hadronic interactions.

the collision without any interaction. This is not the case in the away-side region $\Delta\phi \approx \pi$, suggesting that away-side particles are likely to be lost while traversing the hadronic medium in our simulations.

C. Elliptic flow coefficients

Another way of characterizing heavy-ion collisions is the study of elliptic flow. In traditional hybrid models, elliptic flow arises because of a conversion of geometric anisotropy to a momentum space anisotropy that takes place mostly in a partonic phase. It is usually quantified by the elliptic flow coefficient v_2 , which can be calculated using two-particle cumulants [54, 55] and has been measured extensively by experiments such as ALICE and CMS. When calculated with particle pairs in

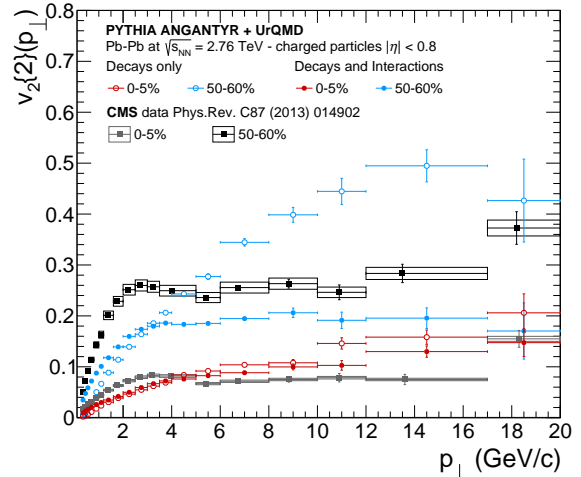


Figure 11. Elliptic flow coefficient v_2 as a function of p_{\perp} in mid-central and central collisions in Pb-Pb at $\sqrt{s_{NN}} = 2.76$ TeV in PYTHIA/Angantyr+UrQMD with and without hadronic interactions compared to data from the CMS experiment [8].

the same rapidity window, the v_2 obtained with cumulants is denoted $v_2\{2\}$ and is affected by dijet correlations.

In PYTHIA/Angantyr, particles are produced incoherently and without any correlation to the event plane, hence no elliptic flow is expected. However, non-flow effects such as correlations of decays, momentum conservation and jets will still produce a measurable $v_2\{2\}$, as seen in Fig. 11. When coupled to UrQMD, the coordinate space anisotropy does get converted into a momentum anisotropy via hadronic interactions at low p_{\perp} , even if this effect is not sufficient to reproduce the measured $v_2\{2\}$, as seen in Fig. 11. This observation is consistent with previous work in which hadronic interactions were observed to lead to a momentum anisotropy in the final state [56].

At high p_{\perp} , where non-flow contributions dominate, the $v_2\{2\}$ obtained with hadronic interactions is significantly lower than the one observed without interactions. This is because dijet correlations are suppressed, as seen in Fig. 8, such that the behavior observed in PYTHIA/Angantyr+UrQMD simulations is more similar to measurements from the CMS collaboration, at least qualitatively. The reduction of the $v_2\{2\}$ is most pronounced in the 50-60% event class, as shown in Fig. 11, as opposed to in the 0-5% class. This observation is due to the fact that in central events, non-flow correlations are so numerous that they are already sufficiently diluted by two-particle combinatorics.

The observation of a non-zero v_2 in PYTHIA/Angantyr+UrQMD with hadronic interactions can be further investigated by looking at further options of calculating the v_2 , as seen

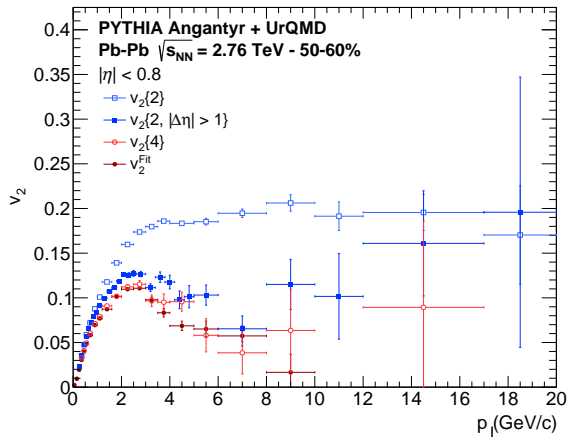


Figure 12. Transverse momentum-differential elliptic flow coefficient v_2 calculated using various methods in Pb-Pb collisions at $\sqrt{s} = 2.76$ TeV. See text for a detailed description.

in Fig. 12. The $v_2\{2\}$ calculated with an eta gap of 1.0 shows a significant reduction of the flow coefficient, especially at high momenta, indicating that short-range two-particle correlations dominate in that regime. This is further corroborated by the values obtained if calculating v_2 using 4-particle cumulants, i.e. the $v_2\{4\}$, which is only slightly smaller than the $v_2\{2, |\Delta\eta| > 1.0\}$, the v_2 obtained with an eta gap. To test if the observed v_2 is correlated with the event plane, we have calculated the v_2 using an alternate method in which the azimuthal particle emission distribution with respect to the event plane is adjusted with a $A + B \cos \Delta\phi$ function, where A and B are free parameters and ϕ is the angle with respect to the event plane. The result is shown as v_2^{Fit} in Fig. 12. The similarity of the v_2^{Fit} with $v_2\{4\}$ indicates that indeed the observed elliptic flow correlates with the event plane direction, as it should also in hydrodynamics simulations, despite the fact that the absolute values are still smaller than data.

D. Studying UrQMD response

Given that the hadronic phase led to a buildup of flow in the PYTHIA-based model, an important question is if this buildup would behave additively in case an initial pre-hadronic-phase flow was present. This is relevant for future inclusion of collective behavior of the system in the pre-hadronization, e.g. string shoving in the PYTHIA/Angantyr model [57, 58]. If the elliptic flow buildup in the hadronic phase is additive with respect to the flow at the beginning of this phase, then an implementation of collective behavior at the partonic phase would only need to account for a fraction of the final-state elliptic flow.

In order to test UrQMD response, we developed

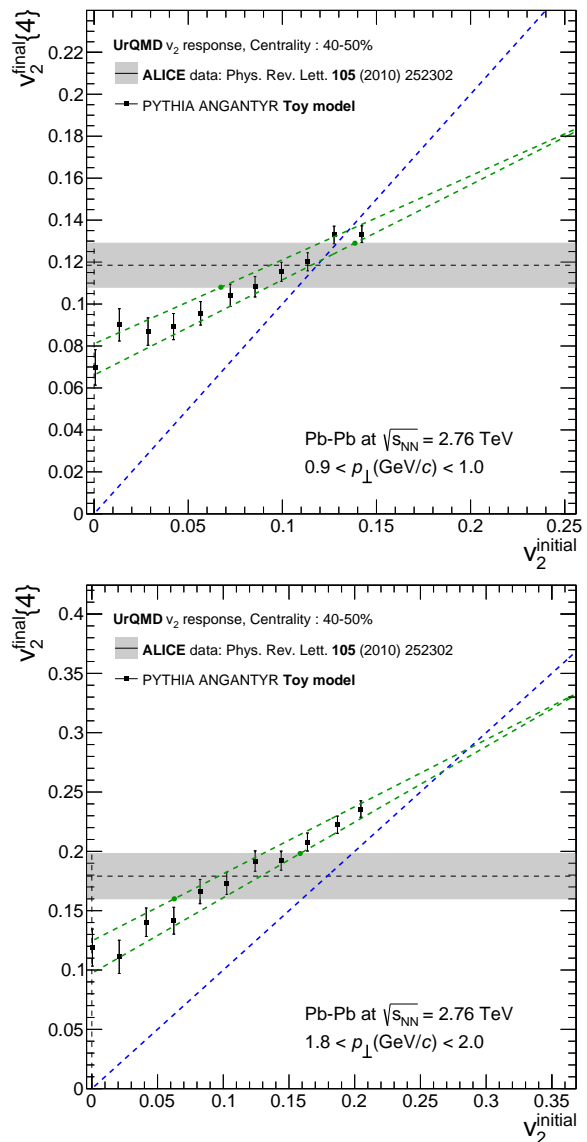


Figure 13. Final-state $v_2\{4\}$ versus pre-hadronic-phase v_2 in the hydrodynamics-based and PYTHIA 8.2-based models for two selected p_T intervals. The black points correspond to setups in which a pre-hadronic-phase v_2^{Fit} was added to PYTHIA/Angantyr output by slightly rotating the hadrons' transverse momentum towards the event plane, as described in the text. The dashed green lines is a linear fit to the minimum and maximum value of $v_2^{\text{Final}}\{4\}$ allowed by the error bars and are used to build Fig .14.

a setup in which the transverse momenta obtained from the PYTHIA/Angantyr generator are rotated before the UrQMD evolution in such a way that a configurable $v_2(p_\perp)$ could be set as desired. This artificial $v_2(p_\perp)$ is introduced following the relation

$$v_2(p_\perp) = \frac{Ap_T}{1 + Bp_\perp(1 + Cp_\perp^2)}, \quad (10)$$

$$B = 0.315 \text{ (GeV/c)}^{-1},$$

$$C = 0.112 \text{ (GeV/c)}^{-2},$$

where A is a parameter that can be freely scaled to obtain various levels of initial flow. The values of B and C were obtained by fitting Eq. 10 to v_2 obtained from the PYTHIA/Angantyr+UrQMD model in the centrality class 40-50%, which exhibits the same momentum dependence as the measured elliptic flow in Pb-Pb collisions while allowing for a fit to be performed in narrow p_\perp intervals. The scale parameter A can be changed to increase or decrease the magnitude of the introduced elliptic flow. We simulated with 11 different values of A and show how the final, post-hadronic-phase $v_2\{4\}$ changes as a function of the v_2 introduced at hadronization time. The gray band shows us the value of $v_2\{4\}$ as computed by the ALICE collaboration in Ref. [59]. Figure 13 indicates that there is a dependence of UrQMD response with respect to the transverse momentum. The rate with which the final-state elliptic flow increases seems to be smaller at low p_T than at high p_T . The result is that the pre-hadronic phase needs to generate almost the same amount of flow as in the experiment in the low- p_T region. But for higher transverse momentum, only 50% of the final state flow needs to be present. A complete study of the allowed range of initial flow (in centrality 40-50%) can be found in Figure 14. This indicates that a model like PYTHIA/Angantyr should generate flow at hadronization time with a weaker dependence of transverse momentum than what is observed experimentally, providing guidance to further PYTHIA/Angantyr developments such as string shoving [58].

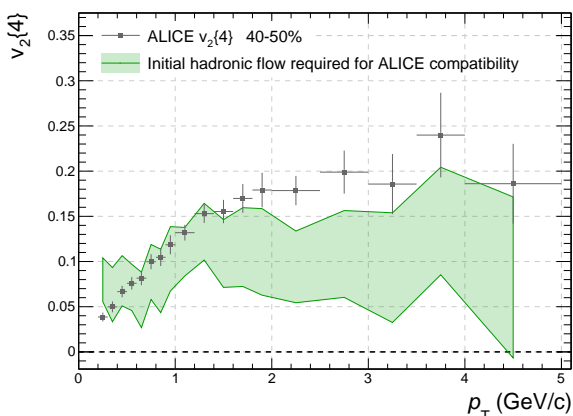


Figure 14. Range of acceptable values that a partonic phase like PYTHIA/Angantyr+UrQMD should have as to reproduce experimental data (green band). We also show the elliptic flow values measured experimentally as reference.

III. CONCLUSION

In this work, we have discussed three basic aspects of PYTHIA/Angantyr+UrQMD simula-

tions: the nuclear modification factor, two-particle correlations and elliptic flow. The fact that the nuclear modification factor calculated using PYTHIA/Angantyr+UrQMD simulations follows the qualitative trend of the measured R_{AA} at intermediate p_\perp once hadronic interactions are considered is an intriguing observation in itself. As explained in the introduction, values for R_{AA} below unity are generally taken as a clear indication of QGP formation, and models incorporating QGP formation are, as a general rule, needed to describe the data. In PYTHIA/Angantyr+UrQMD there is no assumption of a QGP phase, but nevertheless several effects contribute to the description of R_{AA} .

The high- p_\perp part of the spectra generated by PYTHIA/Angantyr deviates from the simple binary scaling which is normally expected [14], as seen also in the fact that the R_{AA} is constant but below unity for high p_\perp even without hadronic interactions. As previously explained, PYTHIA/Angantyr makes a distinction between various types of nucleon-nucleon interactions, which will contribute differently to high- p_\perp particle yields, and as a result the high- p_\perp R_{AA} does not converge to unity even if hadronic interactions are disabled. This effect is responsible for the majority of the deviation from unity, as seen in Fig. 7. There are, however, model uncertainties associated with this effect. While the treatment of secondary absorptive sub-collisions similar to diffractive excitations can be theoretically and numerically motivated [28], it is, as mentioned earlier, not clear that it will exactly reproduce the phenomenology of an interleaved shower plus color reconnection. An obvious next step would be to study the (absence of) nuclear modification in p-Pb collisions within PYTHIA/Angantyr+UrQMD. However, in that case, model uncertainties are much larger than in AA collisions. It was shown in ref. [28] that secondary collisions contribute between 25-40% in Pb-Pb collisions at $\sqrt{s_{NN}} = 2.76$ TeV, while for p-Pb collisions at $\sqrt{s_{NN}} = 5.02$ TeV they contribute between 50-85%.

An equally important conclusion from this work is the influence from the hadronic rescattering phase on R_{AA} . Since strings have an average life-time $\langle \tau^2 \rangle \approx 2$ fm/c, the hadronic phase is longer, and with a more dense initial condition, than for hydrodynamic simulations where a QGP phase lives for up to an order of magnitude longer. We have shown that a hadronic rescattering phase with such an early starting time modifies R_{AA} up to a factor 3 for intermediate p_\perp particles in central Pb-Pb events. From this model, we can interpret that at intermediate p_\perp , hadronic interactions lead to a suppression of particle yields as hadrons lose significant momentum to more abundant low- p_\perp particles. However, this effect subsides for very large transverse momentum, such that the R_{AA} will eventually converge to the value without hadronic interactions. This is because, in

the hadron vertex model, higher- p_{\perp} values correlate with more displaced hadron creation vertices due to the linear relationship between space-time and momentum in Eq. (6), visible also in Fig. 3. Since higher- p_{\perp} particles are then increasingly displaced, these are less likely to interact with the remainder of the system. While this effect is smaller in magnitude than the deviation from binary scaling, it is crucial to recover the minimum of the nuclear modification factor at around 5 GeV/ c and the subsequent rise at high momenta.

It has to be noted that the intermediate to high- p_{\perp} suppression studied in this paper is fundamentally different than the one that would result from models such as JETSCAPE or JEWEL. In the latter, jet quenching is a phenomenon associated to partonic energy loss, which would lead to the suppression of an entire high-momentum jet, while in the former, individual hadrons lose momentum after hadronization. Experimentally, these two scenarios can be distinguished using techniques such as two-particle correlations and dijet asymmetry measurements. It is with this motivation that we pursued the studies shown in Fig. 8, which indicate that the high-momentum particle suppression from hadronic rescattering follows, in fact, again the same qualitative trend as what was observed by the STAR collaboration at RHIC [6, 7], with the near-side jet being mostly unaltered and the away-side jet being suppressed due to a larger number of interactions with the hadronic medium. These findings are complementary to recent studies on the effect of hadronic rescattering on jet shapes [60] which also indicate that the hadronic phase does have significant impact on high- p_{\perp} physics observables.

To further elaborate on the loss of dijet structures at high p_{\perp} , we also calculated the p_{\perp} -differential $v_2\{2\}$ with and without interactions and compared the results to measurements by the CMS collaboration. While the predictions without rescattering overshoot the CMS measurements very significantly, the addition of hadronic interactions reduces the $v_2\{2\}$ very significantly, bringing it closer to CMS data even if the overall magnitude of the $v_2\{2\}$ is underpredicted. Furthermore, we studied UrQMD response by artificially introducing flow at the beginning of the hadronic phase and have shown that, while flow must still be generated during the partonic phase, its over-

all momentum dependence may be milder as the hadronic phase still contributes to the final flow. This observation sets the stage for future developments of the PYTHIA/Angantyr model, notably the inclusion of string shoving [57, 61]. A more comprehensive study of flow coefficients from the PYTHIA/Angantyr+UrQMD model suggests itself as the next step of this work, but lies beyond the scope of this particular manuscript. Another topic of interest that may be pursued in the future is the evolution of identified particle ratios with centrality, in which case inelastic scatterings in the hadronic phase may have a significant impact in high-multiplicity heavy-ion collisions.

We also take this opportunity to highlight further work done to include hadronic rescattering in pp collisions even within the PYTHIA generator itself [62]. A natural extension of these studies would be to use the same machinery in Pb-Pb collisions, which might provide several advantages over UrQMD- for instance, with the possibility of treating also charmed hadrons during the hadronic phase.

The findings of this paper prompt present and future experimental studies to put more emphasis in the construction of baseline, no-QGP models, as a certain fraction of the observations normally exclusively associated with the QGP may have its origin elsewhere. Phrased differently, this work conclusively demonstrates that comparing experimental data with an incoherent superposition of proton-proton collisions is not a valid exercise to fully isolate QGP-specific equilibration signatures.

IV. ACKNOWLEDGEMENTS

We thank Marcus Bleicher for insightful discussions.

The authors would further like to acknowledge support from individual funding bodies: CB was supported by Swedish Research Council, contract number 2017-003. AVS, DDC, WMS and JT were supported by FAPESP project number 17/05685-2 and 2009/54213-0. AVS would also like to acknowledge CAPES for the support under Finance Code 001. This research used the computing resources and assistance of the John David Rogers Computing Center (CCJDR) in the Institute of Physics "Gleb Wataghin", University of Campinas.

[1] K. Adcox *et al.*, "Formation of dense partonic matter in relativistic nucleus-nucleus collisions at RHIC: Experimental evaluation by the PHENIX collaboration," *Nucl. Phys.*, vol. A757, pp. 184–283, 2005.

[2] J. Adams *et al.*, "Experimental and theoretical challenges in the search for the quark gluon plasma: The STAR Collaboration's critical assess-

ment of the evidence from RHIC collisions," *Nucl. Phys.*, vol. A757, pp. 102–183, 2005.

[3] B. B. Back *et al.*, "The PHOBOS perspective on discoveries at RHIC," *Nucl. Phys.*, vol. A757, pp. 28–101, 2005.

[4] I. Arsene *et al.*, "Quark gluon plasma and color glass condensate at RHIC? The Perspective from the BRAHMS experiment," *Nucl. Phys.*,

- vol. A757, pp. 1–27, 2005.
- [5] S. Acharya *et al.*, “Transverse momentum spectra and nuclear modification factors of charged particles in pp, p-Pb and Pb-Pb collisions at the LHC,” *Journal of High Energy Physics*, vol. 2018, Nov 2018.
 - [6] C. Adler *et al.*, “Disappearance of Back-To-Back High- p_T Hadron Correlations in Central Au+Au Collisions at $\sqrt{s_{NN}} = 200$ GeV,” *Physical Review Letters*, vol. 90, Feb 2003.
 - [7] J. Adams *et al.*, “Evidence from $d + Au$ Measurements for Final-State Suppression of High- p_T Hadrons in Au + Au Collisions at RHIC,” *Phys. Rev. Lett.*, vol. 91, p. 072304, Aug 2003.
 - [8] S. Chatrchyan *et al.*, “Measurement of the elliptic anisotropy of charged particles produced in PbPb collisions at $\sqrt{s_{NN}} = 2.76$ TeV,” *Phys. Rev. C*, vol. 87, p. 014902, Jan 2013.
 - [9] V. Khachatryan *et al.*, “Evidence for collectivity in pp collisions at the LHC,” *Phys. Lett.*, vol. B765, pp. 193–220, 2017.
 - [10] J. Adam *et al.*, “Enhanced production of multi-strange hadrons in high-multiplicity proton-proton collisions,” *Nature Phys.*, vol. 13, pp. 535–539, 2017.
 - [11] S. Acharya *et al.*, “Centrality and pseudorapidity dependence of the charged-particle multiplicity density in Xe–Xe collisions at $\sqrt{s_{NN}} = 5.44$ TeV,” *Phys. Lett.*, vol. B790, pp. 35–48, 2019.
 - [12] S. A. Bass *et al.*, “Microscopic models for ultrarelativistic heavy ion collisions,” *Prog. Part. Nucl. Phys.*, vol. 41, pp. 255–369, 1998. [Prog. Part. Nucl. Phys.41,225(1998)].
 - [13] R. J. Glauber, “Cross-sections in deuterium at high-energies,” *Phys. Rev.*, vol. 100, pp. 242–248, 1955.
 - [14] M. L. Miller, K. Reygers, S. J. Sanders, and P. Steinberg, “Glauber modeling in high energy nuclear collisions,” *Ann. Rev. Nucl. Part. Sci.*, vol. 57, pp. 205–243, 2007.
 - [15] S. Cao *et al.*, “Multistage Monte-Carlo simulation of jet modification in a static medium,” *Phys. Rev.*, vol. C96, no. 2, p. 024909, 2017.
 - [16] A. Majumder, “The In-medium scale evolution in jet modification,” 2009.
 - [17] B. Schenke, C. Gale, and S. Jeon, “MARTINI: An Event generator for relativistic heavy-ion collisions,” *Phys. Rev.*, vol. C80, p. 054913, 2009.
 - [18] Y. He, T. Luo, X.-N. Wang, and Y. Zhu, “Linear Boltzmann Transport for Jet Propagation in the Quark-Gluon Plasma: Elastic Processes and Medium Recoil,” *Phys. Rev.*, vol. C91, p. 054908, 2015. [Erratum: Phys. Rev. C97, no. 1, 019902(2018)].
 - [19] K. C. Zapp, “JEWEL 2.0.0: directions for use,” *Eur. Phys. J.*, vol. C74, no. 2, p. 2762, 2014.
 - [20] K. C. Zapp, F. Krauss, and U. A. Wiedemann, “A perturbative framework for jet quenching,” *JHEP*, vol. 03, p. 080, 2013.
 - [21] B. Andersson, G. Gustafson, G. Ingelman, and T. Sjostrand, “Parton Fragmentation and String Dynamics,” *Phys. Rept.*, vol. 97, pp. 31–145, 1983.
 - [22] G. Marchesini and B. R. Webber, “Simulation of QCD Jets Including Soft Gluon Interference,” *Nucl. Phys.*, vol. B238, pp. 1–29, 1984.
 - [23] T. Sjöstrand, S. Ask, J. R. Christiansen, R. Corke, N. Desai, P. Ilten, S. Mrenna, S. Prestel, C. O. Rasmussen, and P. Z. Skands, “An Introduction to PYTHIA 8.2,” *Comput. Phys. Commun.*, vol. 191, pp. 159–177, 2015.
 - [24] J. Bellm *et al.*, “Herwig 7.0/Herwig++ 3.0 release note,” *Eur. Phys. J.*, vol. C76, no. 4, p. 196, 2016.
 - [25] T. Gleisberg, S. Hoeche, F. Krauss, M. Schonherr, S. Schumann, F. Siegert, and J. Winter, “Event generation with SHERPA 1.1,” *JHEP*, vol. 02, p. 007, 2009.
 - [26] T. Sjostrand and M. van Zijl, “A Multiple Interaction Model for the Event Structure in Hadron Collisions,” *Phys. Rev.*, vol. D36, p. 2019, 1987.
 - [27] C. Bierlich, G. Gustafson, and L. Lönnblad, “Diffractive and non-diffractive wounded nucleons and final states in pA collisions,” *JHEP*, vol. 10, p. 139, 2016.
 - [28] C. Bierlich, G. Gustafson, L. Lönnblad, and H. Shah, “The Angantyr model for Heavy-Ion Collisions in PYTHIA8,” *JHEP*, vol. 10, p. 134, 2018.
 - [29] M. Bleicher *et al.*, “Relativistic hadron hadron collisions in the ultrarelativistic quantum molecular dynamics model,” *J. Phys.*, vol. G25, pp. 1859–1896, 1999.
 - [30] J. Weil *et al.*, “Particle production and equilibrium properties within a new hadron transport approach for heavy-ion collisions,” *Phys. Rev. C*, vol. 94, no. 5, p. 054905, 2016.
 - [31] H. Petersen, J. Steinheimer, G. Burau, M. Bleicher, and H. Stocker, “A Fully Integrated Transport Approach to Heavy Ion Reactions with an Intermediate Hydrodynamic Stage,” *Phys. Rev.*, vol. C78, p. 044901, 2008.
 - [32] D. Heck, J. Knapp, J. N. Capdevielle, G. Schatz, and T. Thouw, “CORSIKA: A Monte Carlo code to simulate extensive air showers,” 1998.
 - [33] S. Agostinelli *et al.*, “GEANT4: A Simulation toolkit,” *Nucl. Instrum. Meth.*, vol. A506, pp. 250–303, 2003.
 - [34] R. D. Weller and P. Romatschke, “One fluid to rule them all: viscous hydrodynamic description of event-by-event central p+p, p+Pb and Pb+Pb collisions at $\sqrt{s} = 5.02$ TeV,” *Phys. Lett.*, vol. B774, pp. 351–356, 2017.
 - [35] MPIs are not fully independent, as 1) the parton density function corresponding to an extracted parton is rescaled by a factor $(1 - x)$, and 2) the full collision has to conserve energy and momentum.
 - [36] R. Corke and T. Sjostrand, “Interleaved Parton Showers and Tuning Prospects,” *JHEP*, vol. 03, p. 032, 2011.
 - [37] A. Bialas, M. Bleszynski, and W. Czyz, “Multiplicity Distributions in Nucleus-Nucleus Collisions at High-Energies,” *Nucl. Phys.*, vol. B111, pp. 461–476, 1976.
 - [38] B. Andersson, G. Gustafson, and B. Nilsson-Almqvist, “A Model for Low p(t) Hadronic Reactions, with Generalizations to Hadron - Nucleus and Nucleus-Nucleus Collisions,” *Nucl. Phys.*, vol. B281, pp. 289–309, 1987.
 - [39] C. Bierlich, G. Gustafson, L. Lönnblad, and A. Tarasov, “Effects of Overlapping Strings in pp Collisions,” *JHEP*, vol. 03, p. 148, 2015.
 - [40] C. Bierlich, G. Gustafson, and L. Lönnblad, “Collectivity without plasma in hadronic collisions,”

- Phys. Lett.*, vol. B779, pp. 58–63, 2018.
- [41] B. Andersson, G. Gustafson, and B. Soderberg, “A General Model for Jet Fragmentation,” *Z. Phys.*, vol. C20, p. 317, 1983.
- [42] B. Andersson, “The Lund model,” *Camb. Monogr. Part. Phys. Nucl. Phys. Cosmol.*, vol. 7, pp. 1–471, 1997.
- [43] T. Sjostrand, “Jet Fragmentation of Nearby Partons,” *Nucl. Phys.*, vol. B248, pp. 469–502, 1984.
- [44] G. S. Bali, “Casimir scaling of SU(3) static potentials,” *Phys. Rev.*, vol. D62, p. 114503, 2000.
- [45] For more details about fragmentation dynamics, the reader is referred to refs. [21, 41–43], as well as ref. [23] for a more recent review.
- [46] P. Skands, S. Carrazza, and J. Rojo, “Tuning PYTHIA 8.1: the Monash 2013 Tune,” *Eur. Phys. J.*, vol. C74, no. 8, p. 3024, 2014.
- [47] S. Ferreres-Solé and T. Sjöstrand, “The space-time structure of hadronization in the Lund model,” *Eur. Phys. J.*, vol. C78, no. 11, p. 983, 2018.
- [48] K. Aamodt *et al.*, “Centrality dependence of the charged-particle multiplicity density at mid-rapidity in Pb-Pb collisions at $\sqrt{s_{NN}} = 2.76$ TeV,” *Phys. Rev. Lett.*, vol. 106, p. 032301, 2011.
- [49] S. Acharya *et al.*, “Transverse momentum spectra and nuclear modification factors of charged particles in pp, p-Pb and Pb-Pb collisions at the LHC,” *JHEP*, vol. 11, p. 013, 2018.
- [50] “Centrality determination in heavy ion collisions,” *ALICE-PUBLIC-2018-011*, 2018.
- [51] K. J. Eskola, K. Kajantie, and J. Lindfors, “Quark and Gluon Production in High-Energy Nucleus-Nucleus Collisions,” *Nucl. Phys.*, vol. B323, pp. 37–52, 1989.
- [52] J. Ranft, “Hadron Production in Hadron - Nucleus and Nucleus-nucleus Collisions in the Dual Monte Carlo Multichain Fragmentation Model,” *Phys. Rev.*, vol. D37, p. 1842, 1988.
- [53] We note that there is a similar agreement between PYTHIA/Angantyr+UrQMD and data for R_{AA} measured in Xe-Xe collisions at $\sqrt{s_{NN}} = 5.44$ TeV, making a complete co-incidence unlikely.
- [54] N. Borghini, P. M. Dinh, and J.-Y. Ollitrault, “New method for measuring azimuthal distributions in nucleus-nucleus collisions,” *Phys. Rev. C*, vol. 63, p. 054906, Apr 2001.
- [55] N. Borghini, P. M. Dinh, and J.-Y. Ollitrault, “Flow analysis from multiparticle azimuthal correlations,” *Phys. Rev. C*, vol. 64, p. 054901, Sep 2001.
- [56] Y. Lu, M. Bleicher, F. Liu, Z. Liu, H. Petersen, P. Sorensen, H. Stöcker, N. Xu, and X. Zhu, “Anisotropic flow at RHIC: how unique is the number-of-constituent-quark scaling?,” *J.Phys.G: Nuclear and Particle Physics*, vol. 32, p. 1121–1129, Jun 2006.
- [57] C. Bierlich, G. Gustafson, and L. Lönnblad, “A shoving model for collectivity in hadronic collisions,” 12 2016.
- [58] C. Bierlich, S. Chakraborty, G. Gustafson, and L. Lönnblad, “Setting the string shoving picture in a new frame,” 10 2020.
- [59] K. Aamodt *et al.*, “Elliptic flow of charged particles in Pb-Pb collisions at 2.76 TeV,” *Phys. Rev. Lett.*, vol. 105, p. 252302, 2010.
- [60] P. Dorau, J.-B. Rose, D. Pablos, and H. Elfner, “Jet quenching in the hadron gas: An exploratory study,” *Physical Review C*, vol. 101, Mar 2020.
- [61] L. Lönnblad, “Modelling pp, pA and AA in Pythia8,” *EPJ Web Conf.*, vol. 208, p. 11003, 2019.
- [62] T. Sjöstrand and M. Uthheim, “A framework for hadronic rescattering in pp collisions,” 2020.